Spectroscopic investigation of fast (ns) magnetic field penetration in a plasma*

M. Sarfaty, R. Shpitalnik, R. Arad, A. Weingarten, Ya. E. Krasik, A. Fruchtman, and Y. Maron†
Department of Particle Physics, Weizmann Institute of Science, Rehovot 76100, Israel

(Received 17 November 1994; accepted 1 March 1995)

The time-dependent magnetic field spatial distribution in a coaxial positive-polarity plasma opening switch (POS) carrying a current ≃135 kA during ≃100 ns, was investigated by two methods. In the first, ionic line emission was observed simultaneously for two polarizations to yield the Doppler and Zeeman contributions to the line profiles. In the second method, the axial velocity distribution of ions was determined, giving the magnetic field through the ion equation of motion. This method requires knowledge of the electron density, here obtained from the observed particle ionization times. To this end, a lower bound for the electron kinetic energy was determined using various line intensities and time-dependent collisional-radiative calculations. An important necessity for POS studies is the locality of all measurements in r, z, and θ. This was achieved by using laser evaporation to seed the plasma nonperturbingly with the species desired for the various measurements. The Zeeman splitting and the ion motion showed magnetic field penetration through the 3.5 cm long plasma at a velocity $\simeq 10^8$ cm/s. The current density was found to be relatively high at the load-side edge of the switch plasma. It is suggested that this may cause plasma acceleration into the vacuum section toward the load, which is supported by charge-collector measurements. The fast magnetic field penetration agrees with estimates based on the Hall-field mechanism. © *1995 American Institute of Physics.*

I. INTRODUCTION

Investigating the behavior of plasmas carrying high short-duration currents is of major importance for improving the understanding of fundamental plasma physics phenomena, such as magnetic field penetration into plasmas and plasma flow under magnetic and electric fields. Such studies are also essential for improving and scaling up of many pulsed-power systems.

In previous studies, information on the evolution of the magnetic field in plasma opening switches (POS) was obtained by the use of magnetic loops inserted in the plasma.[1] Recently, the time-dependent line-integrated plasma electron density, was studied in a microsecond POS using laser interferometry.[2] More experimental investigations are highly required for studying the plasma behavior in plasma opening switches and for examining the various underlying theories.[3–7]

The question of the magnetic field penetration into short-duration plasmas is of major importance for many pulsed-power systems. In particular in POS, the magnetic field affects both the plasma properties in the conduction phase and the switch opening. Field penetration due to diffusion appears unlikely since the classical diffusion time is >500 times longer than the pulse duration (100 ns) and instability-induced resistivity is presumably not sufficiently high to allow for diffusion in such a time scale.[8] Recently developed theories based on the Hall effect raise possibilities for fast penetration.[5,6] The motivation for this work was the development of nonintrusive methods for time-dependent and spatially resolved measurements to determine the magnetic field distribution in the plasma.

In POS research, because of the transient nature of the phenomena and of the atomic-physics processes, performing local measurements is essential for achieving reasonably unambiguous results. To this end, we developed a method to seed the plasma locally with various species desired for the various spectroscopic observations. For this technique, it is required to verify that the seeded species do not affect the plasma electron density and temperature, which was verified by various spectroscopic observations. This technique allowed for local measurements in r, z, and θ, of the magnetic field, particle velocities, electron density, and electron kinetic energy.

For this study, a gaseous plasma source[9,10] was developed in order to allow the plasma composition to be controlled with satisfactory reproducibility and uniformity. The source is mounted inside the inner high-voltage electrode and injects the plasma radially outwards into the interelectrode gap. Knowledge of the electron density and temperature of the source plasma, together with the particle velocity distributions, prior to the current pulse is found to be of high importance for interpreting the observations during the pulse. These parameters were determined by spectroscopic and other techniques.[9]

In this paper we present results of the magnetic field distribution measured using two methods. In the first, the magnetic field intensity was obtained from spectral line profiles affected by Zeeman splitting.[11] The second method relies on determining the particle velocity distributions from Doppler-dominated line profiles and the electron density from ionization times of particles seeded in the plasma. The magnetic field distribution is then calculated from the ion

*Paper 1IB1, Bull. Am. Phys. Soc. **39**, 1517 (1994).
†Invited speaker.

 1070-664X/95/2(6)/2583/7/$6.00

equation of motion. We also obtained a lower limit of a few tens of electron-volts for the electron energy from level populations into the plasma. A relatively high current density at the load-side edge of the plasma is inferred.

II. THE EXPERIMENTAL SETUP AND DIAGNOSTICS

A. The plasma opening switch

In this study we use a coaxial POS with anode and cathode radii of 2.5 cm and 5.0 cm, respectively. The POS upstream inductance is 120 nH and the load is a shorted coaxial line with an inductance of 25 nH. A positive high-voltage pulse (4.1 kJ, 300 kV, 1 Ω), delivered by an LC-water-line generator, gives a peak current of 135 ± 10 kA with a quarter period of 90 ns. Two calibrated Rogowski coils and two sets of four $\dot{B}$ loops azimuthally separated by 90° are used to measure the upstream and downstream currents and the current azimuthal symmetry.

The plasma source is installed inside the inner POS electrode and injects the plasma radially outward into the anode–cathode (A–K) gap through a 75% transparent stripped cylindrical anode. In the plasma gun, the plasma is produced in 144 alumina-made capillaries filled with gas. The capillaries are placed radially in the walls of a hollow cylindrical tube. In the present measurements CH_4 was used, forming a plasma composed of carbon ions, protons, and neutral particles. The plasma parameters prior to the current pulse were determined from electric probes measurements, microwave cutoff data, and observations of H_α and H_β spectral profiles. The electron temperature and density at 0.5 cm from the anode were found to be 2 ± 1 eV and $(1.5\pm0.3)\times10^{14}$ cm^{-3}, respectively. The density is about half that at 0.5 cm from the cathode. The plasma axial length is $\simeq$3.5 cm at a distance 0.5 cm from the anode. The axial density uniformity is $\pm15\%$, and the reproducibility is $\pm20\%$. A detailed description of the POS and the plasma source properties is given in Refs. 9 and 10.

B. The diagnostic system

The POS chamber has optical windows that allow axial and radial lines of sight. The spectroscopic setup, shown in Fig. 1, consists of two 1 m spectrometers each equipped with a 2400 grooves/mm grating giving a spectral resolution $\simeq$0.06 Å. The mirrors M1 and M3 are used to scan in different experiments the POS anode–cathode gap radially and axially. The beam splitter allows the two spectrometers to collect light in a single discharge from the same volume element. The cylindrical lenses image the light at the spectrometer exit windows on rectangular fiber-bundle arrays, enabling us to vary the light dispersion in the experiments. Each fiber-bundle array transmits the light to a set of 10 photomultiplier tubes followed by a multichannel digitizer, recording the time-dependent line spectral profile in a single discharge with a temporal resolution of 4 ns. Both spectroscopic systems were absolutely calibrated over the spectral region of 2000–7500 Å. Polarization-dependent measurements were performed using a $\lambda/2$ plate and the inherent polarization of the gratings.

In order to obtain satisfactory spatial resolution along the line of sight we used a pulsed laser (Nd:YAG, 20 ns, 50 mJ per pulse, 2×10^9 W/cm^2 at $\lambda\simeq1.06$ μm) to evaporate material initially deposited on the anode strips into the POS region. This enabled us to seed the plasma with particles desired for the various measurements. The laser pulse is applied $\simeq2$ μs prior to the high current pulse producing a conical column between the POS electrodes with a diameter that increases from $\simeq$0.2 cm near the anode to $\simeq$1 cm in the middle of the POS gap. The axial location of the seeded column was varied in the experiments by moving the laser beam spot on the anode strip. The spatial resolution in the z direction is determined by the seeded-column width, and that in the r and θ directions, $\simeq$0.05 cm and $\simeq$0.5 cm, respectively, by the imaging optics. Various spectroscopic observations were used to verify that during the time of interest the plasma seeding did not alter significantly the electron density and temperature of the preformed plasma.

III. EXPERIMENTAL RESULTS

A. Magnetic field distribution

The magnetic field distribution in the plasma was determined from the Zeeman splitting of line emissions of BaII ions seeded in the plasma. The relatively heavy BaII species was selected for these measurements in order to minimize the Doppler broadening. Nevertheless, observing the Zeeman effect required discrimination against the contribution of the Doppler broadening to the line spectral profile. To this end, by splitting the collected line emission into two spectrometers, the π and σ components of the line profile, from the same volume element in the plasma, were determined separately as a function of time in a single discharge, as shown in Fig. 1.

An example of the profiles of the BaII 6142 Å $[6p(^2P^0)-5d(^2D)]$ line, observed for the two orthogonal polarizations at 0.5 cm from the anode and at an axial position $z=-0.8$ cm, where $z=0$ is the axial center of the switch and positive distance is toward the load, is shown in Fig. 2. Such line profiles were analyzed self-consistently to unfold the Zeeman splitting and the Doppler broadening (the π emission is mainly affected by the Doppler effect).

The ionization of BaII limited these measurements to times up to $\simeq$60 ns after the start of the current pulse. In Fig. 3 we present the magnetic field at different times measured at various axial locations in the plasma at 0.5 cm from the anode. The magnetic field is seen to penetrate the plasma within the first $\simeq$30 ns of the current pulse. Using the $\simeq$3.5 cm plasma length, this gives a penetration velocity $\simeq10^8$ cm/s.

B. Particle velocities

The particle directed velocities and velocity distributions were obtained from Doppler-dominated spectral profiles of various emission lines. A few lines from the same species were used to verify the predominance of the Doppler effect on the line profiles. Each of the measurements was averaged over a few discharges to reduce the experimental uncertainty.

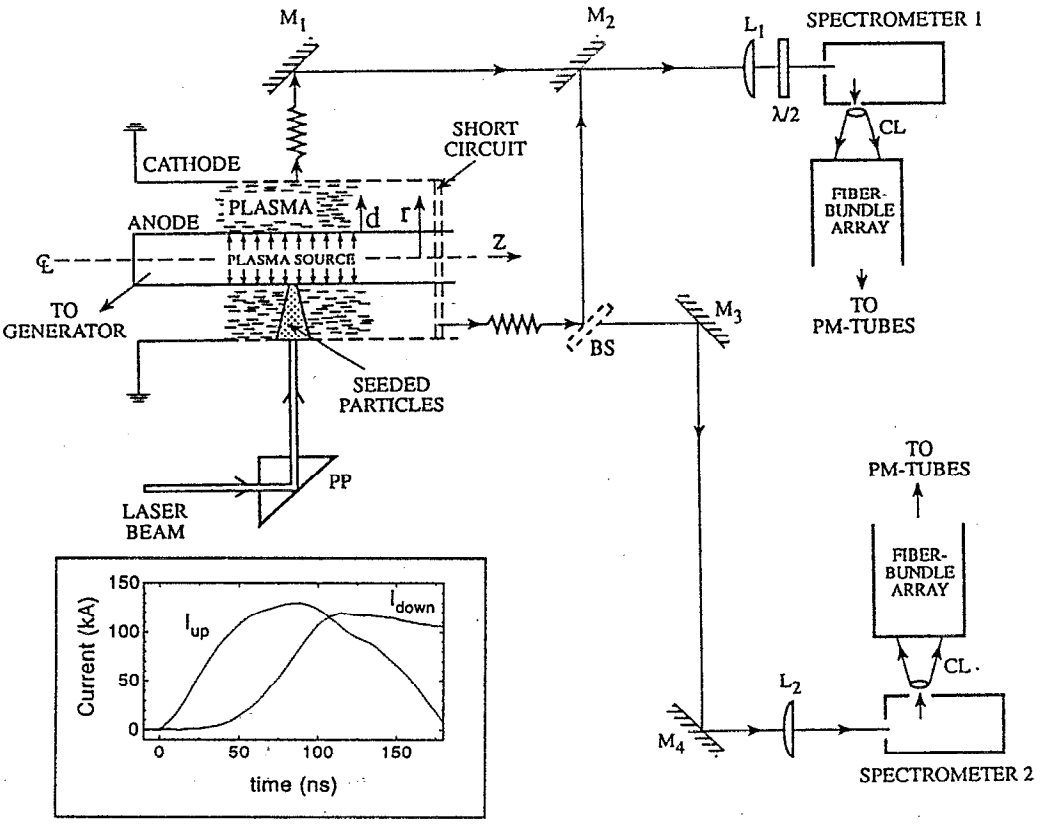

FIG. 1. The diagnostic systems used for the experiments. Light from the plasma is collected axially or radially, and is directed onto the spectrometers by the use of the beam splitter BS, the mirrors M_1, M_2, M_3, and M_4 and the lenses L_1 and L_2. The $\lambda/2$ plate rotates the light polarization to the efficient direction of the gratings. The light at the exit window is optically dispersed using the cylindrical lenses CL and is projected onto rectangular optical-fiber arrays. The signal transmitted through each fiber bundle is measured by a photomultiplier tube. The laser beam used to evaporate material from the anode surface is directed onto the anode via the prism PP that is used to vary, in different experiments, the axial location of the laser beam spot on the anode. The dotted area shows the column of the seeded particles. The insert shows typical upstream and downstream current traces.

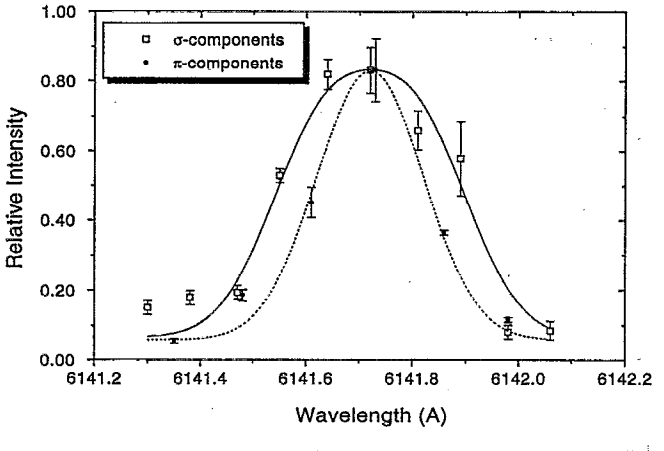

FIG. 2. An example of the σ- and π-polarized line profiles obtained in axial observations of the BaII 6141.7 Å $[6p(^2P^0)-5d(^2D)]$ line. The data are given for 0.5 cm from the anode at $t=40$ ns for $z=-0.8$ cm with respect to the switch center, where positive z denotes distance toward the load. The solid and dashed curves are the line profiles for the σ and π polarizations, respectively, calculated assuming a Gaussian profile for each of the line spectral components. The line width difference corresponds to a 6 kG magnetic field.

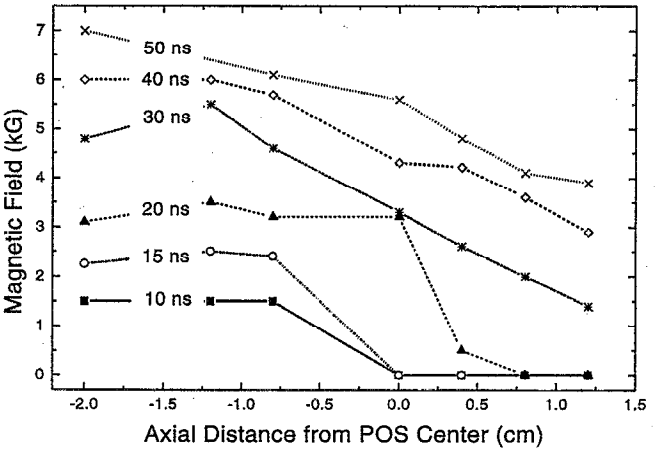

FIG. 3. Axial magnetic field distributions for several times at 0.5 cm from the anode surface obtained from the Zeeman splitting of the BaII 6141.7 Å line. The data points, connected by straight lines, were obtained from fits to the data as in Fig. 2. The uncertainty in the magnetic field amplitude is $\approx\pm 25\%$. The data points at -2 cm are obtained from the upstream current measured by a Rogowski coil. Time $t=0$ corresponds to the beginning of the generator current pulse.

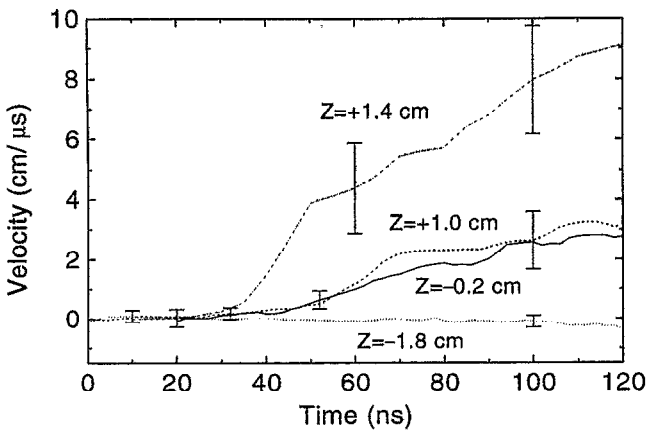

FIG. 4. The time-dependent mean axial MgII velocities obtained from the Doppler shifts of the MgII 2796 Å line at 0.7 cm from the anode. Given are results for the axial locations: $z=-1.8$ (close to the generator-side edge of the plasma), -0.2, $+1.0$, and $+1.4$ cm, where $z=0$ is the axial center of the switch. For the axial position $z=+1.4$ cm (the load-side edge of the plasma) only the fast velocity component is shown. The velocity of the slow component is similar to the one shown for $z=+1.0$ cm.

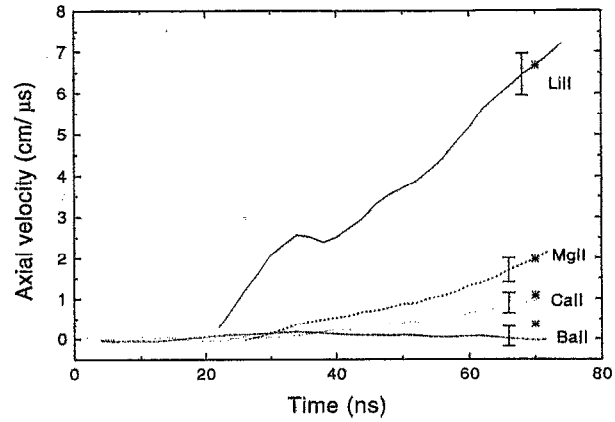

FIG. 5. The time-dependent mean axial velocities of LiII, MgII, CaII, and BaII obtained from the Doppler shifts of their observed lines. The data given are for the axial center of the switch and 0.7 cm from the anode. The stars indicate the expected velocities relative to LiII based on scaling inversely proportional to the ion mass.

Here we present the velocities of MgII particles seeded in the plasma, observed in the axial direction. First, the densities of MgI and MgII were determined from the observed line intensities and collisional-radiative calculations. It was found that the MgI density is five times lower than the MgII density, thus the MgI ionization into MgII has little effect on the evolution of the MgII velocities during the pulse. The axial MgII velocities were determined for ten different axial locations of the seeded-MgII column. In Fig. 4, we present the directed axial velocities of MgII as a function of time for four axial positions at 0.7 cm from the anode. These velocities were obtained from the absolute shifts of the 2796 Å ($3p$-$3s$) line. Positive sign denotes velocities toward the load.

It is seen in Fig. 4 that the ion motion starts within the first 40 ns of the generator pulse at all axial locations across the plasma. At the generator-side edge of the plasma ($z=-1.8$ cm) the directed velocity remains low, while in the central region (-1.4 cm$\leq z\leq+1.0$ cm) it rises to $\simeq 2$ cm/μs at $\simeq 100$ ns. At the load-side edge of the plasma ($z=+1.4$ cm) two distinct ion velocity components were observed. One component has a velocity similar to the one observed in the central region (not shown in Fig. 4), and the other is $\simeq 3$ times faster. The observed slow and fast ion components had similar emission intensities, i.e., about half of the seeded column ($\simeq 0.5$ cm) at the load-side edge of the plasma moves toward the load with the higher velocity. The MgII velocities were also measured at 0.2 cm and 1.7 cm from the anode showing phenomena similar to those found at 0.7 cm. Also, axial velocities for LiII, CaII, and BaII ions were observed at various axial locations. The temporal behavior is similar to that of the MgII ions, including the high velocity component seen near the load-side edge of the plasma. Figure 5 shows the time-dependent axial velocities for these ions at 0.7 cm from the anode at the axial center of the switch. It is seen that the ion velocities are nearly inversely proportional to the ion mass.

We also determined the axial velocities of neutral carbon and carbon ions up to the fourth ionization stage. However, these measurements were integrated along the plasma axial length (i.e., no seeding was used). For CI the velocity at $t=100$ ns was found to remain ≤ 0.5 cm/μs, which is its value prior to the current pulse, while the velocities of CII, CIII, CIV, and CV rose to 1.5, 3.0, 5.0, and 7.0 cm/μs, respectively. To within the measurement accuracy, the velocities were found to scale linearly with the ion charge.

The observed carbon-ion velocities, even though integrated over the entire plasma length, also showed a small fraction of higher velocities. The fraction of these fast ions is consistent with the fast fraction at the load-side edge of the plasma seen in the axially resolved measurements (see Fig. 4).

Radial ion velocities were observed using radial lines of sight at various axial locations. The velocities obtained in this manner are integrated along the radial dimension of the plasma. The measured radial velocities of CI to CV toward the cathode were found to be similar to the axial velocities toward the load.

C. Electron energy and density

A lower bound for the electron kinetic energy was obtained by observing intensities of lines emitted from various transitions of the plasma constituents and seeded particles. In Fig. 6 we show the population of the LiII $2p$ ($^3P^0$) level (lying at $\simeq 61$ eV) derived from the absolute intensity of the 5485 Å line. It is seen that the line intensity at the axial center of the switch and 0.7 cm from the anode starts rising at $t\simeq 20$ ns and reaches nearly a plateau at $t\simeq 60$ ns. Using our collisional-radiative model for lithium and an upper limit for the LiII density in the plasma, $\leq 5\times 10^{13}$ cm^{-3}, we concluded that the mean electron energy $\mathscr{E}_e$ rises at this time to at least $\simeq 50$ eV.

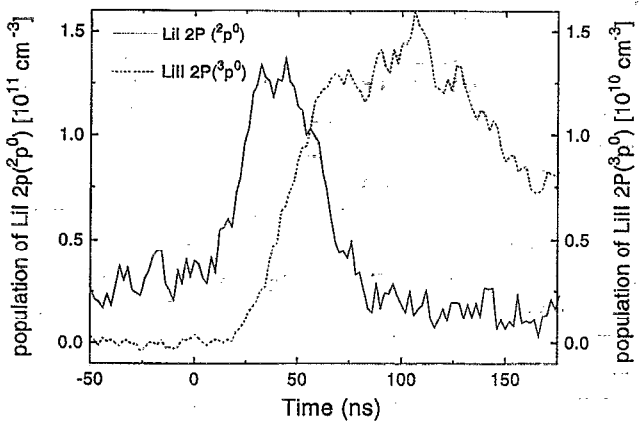

FIG. 6. The time-dependent population densities of the LiI $2p$ level and the LiII $2p$ ($^3P^0$) level, obtained from axial observations of the LiI 6708 Å ($2p-2s$) and the LiII 5485 Å [$2p(^3P^0)$-$2s(^3S)$] line intensities, respectively. The data given are for the axial center of the switch and 0.7 cm from the anode.

The near constancy of the LiII $2p$ ($^3P^0$) level population at $t \gtrsim 60$ μs implies that $\mathscr{E}_e$ remains high up to $t \simeq 100$ ns [it is shown in Ref. 9 that ionization of LiI into LiII or excitations from the nearby metastable level could not substantially affect the LiII $2p$ ($^3P^0$) level density]. The rise in the electron energies was also evident from the observed line intensities of other seeded particles such as LiI, MgI, MgII, CaI, CaII, BaI, and BaII, which require excitation energies of a few electron-volts, as well as from the rise in the line emission of the preformed plasma constituents.

The lower bound of a few tens of electron-volts obtained for the electron energy means that the ionization times of species which have ionization potentials of a few eV are insensitive to the electron energy. The ionization times of such species could, therefore, be used to determine the electron density. To this end, and in order to obtain local measurements, the plasma was seeded with LiI, BaI, BaII, MgI, and CaI. The ionization of LiI, for example, as studied from the population of the LiI $2p$ level during the pulse obtained from the $2p$-$2s$ line intensity. Such a measurement at 0.7 cm from the anode and at the axial center of the switch is shown in Fig. 6. It is seen that the line intensity rises, due to the rise in the mean electron energy, and then decays. In principle, this decay could result from a drop in the electron or ion densities. However, this possibility was excluded by observing line intensities of species that ionize negligibly during the pulse (LiII, MgII, and BaIII), showing no intensity decrease at this period of time. Thus, we conclude that the observed drop in the line intensities of LiI, BaII, MgI, and CaI results from ionization, allowing us to determine the local electron density.

Using the ionization times of these species, the electron density at 0.2–1.0 cm from the anode and along the 3.5 cm long plasma was determined to be $1.3\pm0.5\times10^{14}$ cm^{-3}. Due to limited line intensities, the electron density was determined for $t=20-70$ ns at $z \lesssim 0$ and for $t=60-100$ ns at $z \gtrsim 0$. The uncertainty in n_e mainly results from the irreproducibility in the line intensity time dependence. Note, that the electron density thus obtained is consistent with that measured prior to the current pulse.

IV. DISCUSSION

The direct measurements of the magnetic field from Zeeman splitting of the BaII line at 0.5 cm from the anode surface show a penetration of the magnetic field into the plasma within $\simeq$30 ns after the start of the current pulse followed by a continuous rise of the magnetic field. The ionization of BaII limited these measurements to $t \lesssim 60$ ns. To complement these measurements for later times we used lighter ions whose ionization times are longer. The larger Doppler contribution to the line profiles of these ions allowed their axial velocities to be measured and, together with observed electron density, this allowed the magnetic field distribution to be obtained.

The relatively low ion velocities observed support the early penetration of the magnetic field into the plasma, concluded from the Zeeman-splitting measurements. If the magnetic field did not penetrate, the magnetic field pressure would be expected to push the plasma boundary with a velocity comparable to the Alfvén velocity. For our plasma, mainly composed of protons and carbon ions with a total electron density $\simeq 1.3\times10^{14}$ cm^{-3}, this velocity is estimated to be $\simeq$50 cm/μs. The lower ion velocities observed thus support the fast magnetic field penetration, which results in a lower magnetic field pressure per unit mass of the plasma.

The start of the ion motion over the entire plasma within the first 40 ns of the pulse further supports the field penetration into the plasma at this period of time. Furthermore, the nearly linear dependence of the ion velocities on the charge-to-mass ratio provides additional evidence that the ion motion is due to the Hall field in the plasma resulting from the field penetration.

Assuming that the ions are accelerated by the Hall electric field we now determine the axial magnetic field distribution from the observed local ion velocities. If a current flows through a region in the plasma, the mean axial velocity of ions of mass M and charge Ze in this region satisfies

$$\frac{dV_z}{dt} = \frac{Z}{M}\frac{1}{8\pi\delta n_e}(B_1^2 - B_2^2). \tag{1}$$

Here, B_1 and B_2 are the magnitude of the magnetic field at the axial boundaries of the region, δ is the width of the region, and n_e is the electron density. The derivation of Eq. (1) is obtained from an axial integration of the ion equation of motion over the region, in which the plasma pressure is much smaller than the magnetic field pressure.

We use the axial velocities at different axial positions and Eq. (1) to calculate the magnetic field distribution at various times at 0.7 cm from the anode. At each time $t=60$, 80, and 100 ns, the magnetic field distribution is calculated as follows. The plasma is divided axially into intervals. The acceleration at each interval is estimated from the axial velocities observed at each z, such as those given in Fig. 4. Using the measured density of $n_e \cong 1.3\times10^{14}$ cm^{-3}, we calculate the change in B^2 across each interval. Then, starting from the generator side, where the magnetic field B_{up} is ob-

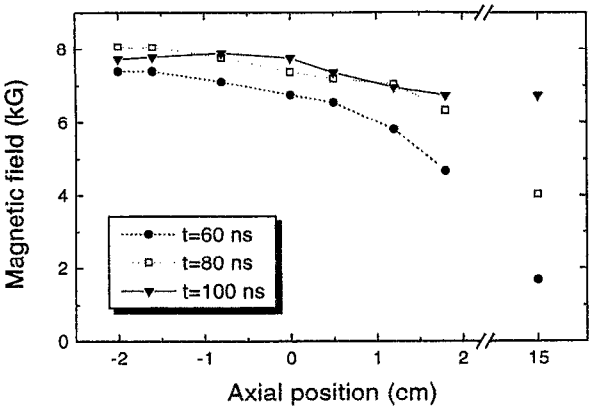

FIG. 7. Axial magnetic field distributions for several times at 0.7 cm from the anode surface obtained from the axial time-dependent local MgII velocities. For the calculation we used the measured electron density 1.3×10^{14} cm^{-3}. The data points are connected by straight lines. The points at $z=-2$ and $+15$ cm give the magnetic field obtained from the upstream and downstream currents, respectively, measured by Rogowski coils.

tained from the upstream current, we calculate B across the plasma. Note that the MgII displacement during the conduction time is small relative to the length of the intervals due to the low MgII velocities. The magnetic field distribution in the plasma thus obtained for various times is shown in Fig. 7. A formation of relatively high current density can be seen for $t\simeq60$ ns at the load-side edge of the plasma, indicated by the larger slope of $B(z)$.

The observed magnetic field penetration into the plasma is at least 500 times faster than expected for a classical diffusion. Assuming the penetration does not result from very high anomalous resistivity, we suggest that the penetration is due to the recently studied[5–7] Hall-field mechanism. The estimated Hall penetration time of $\simeq40$ ns is consistent with our experimental results.

The high current density at the load-side edge of the plasma suggests that plasma from this region can be accelerated into the vacuum section toward the load. The fastest motion is expected for the proton component in this plasma region. Collimated Faraday-cup measurements[10] of the axial plasma flow into the vacuum section yielded a proton flux and velocity consistent with the thickness of the high-current-density edge of the plasma and with the accelerating forces due to the current density there.

For the Hall-field mechanism to be effective the plasma length must be smaller than the ion skin depth, and $n_e r^2$ must increase along the electron path. These conditions are only marginally satisfied in our experiment. More studies of the electron density distribution in the radial and axial directions are required for understanding the field penetration in terms of the Hall effect. In relation to this, we mention the study of Fruchtman and Gomberoff,[6] who suggested possible field penetration in positive-polarity switches. Also, Fruchtman and Rudakov[7] have shown that the plasma pushing by the magnetic field could modify the plasma density in a way that it would become favorable for penetration.

An important question is that of the magnetic field energy dissipation. Because of the fast penetration, only a small part of the dissipated energy is expected to be converted to ion kinetic energy. The predicted low ion kinetic energy is consistent with our experimental data. Most of the dissipated magnetic field energy is expected to become electron kinetic energy. The dissipation per particle expected from the magnetic field penetration is approximately $B^2/8\pi n_e$. It has been recently demonstrated[7] that during the magnetic field penetration the magnetic field energy can be dissipated by accelerating electrons in the current channel to a high energy, and these energetic electrons deposit their energy at the anode. The energetic electrons are only located in the narrow current channel, making their relative number small, while most of the electrons, which remain in the plasma behind the current channel, have lower energies. This theory,[7] therefore, may provide an explanation to the question of energy dissipation. The general feature of accelerating the plasma electrons to the anode and replacing them by relatively cold electrons from the cathode thus providing a way of magnetic field energy dissipation with no electron heating in a collisionless plasma, has also been pointed out by Mendel.[12] Further quantitative investigations of the electron energy distributions, in particular the possible presence of energetic electrons, should be made.

As shown in Fig. 7, the magnetic field at the load-side edge of the plasma obtained from the ion velocities is larger than the magnetic field B_d at the load obtained from the measured downstream current. The difference in these values of the magnetic field probably results from current through plasmas or electron flow in the vacuum section between the plasma edge and the load. We emphasize that the uncertainties in the ion velocities, the electron density, and the width of the high-current-density layer in the load-side edge of the plasma do not allow us to determine accurately the magnitude of the current that flows in the vacuum section.

V. SUMMARY

In this study we presented determination of the magnetic field distribution in a coaxial POS by the observation of the Zeeman effect on spectral line profiles of ions seeded in the plasma. The magnetic field distribution was also obtained from measurements of the local ion directed velocities. The required electron density was obtained from the ionization times of various seeded species whose ionization times are insensitive to the details of the electron energy distribution. The electron energy was studied using line intensities and time-dependent collisional-radiative calculations. The Zeeman measurements show fast magnetic field penetration into the plasma within the first 30 ns of the current pulse, yielding a magnetic field penetration velocity of $\simeq10^8$ cm/s. This is supported by the early start of the ion motion at all axial locations, the relatively low ion velocities, and the nearly linear dependence of the ion velocity on the charge-to-mass ratio. The high ion velocities at the load-side edge of the plasma imply the presence of a relatively high current density at this location.

The question of energy dissipation is most probably connected to the kinetic energy of the electrons. Our measurements so far provided only a lower bound of a few tens of

electron-volts on the electron energy. Further studies are needed in order to estimate the total electron kinetic energy.

ACKNOWLEDGMENTS

The authors are grateful to Dr. A. Fisher for helpful discussions and his invaluable contribution in developing the plasma source. Thanks are due to S. Shkolnikov and Yu. Ralchenko for considerable assistance in the data analysis and to B. Pereiaslovets for his help in the experiments.

This work was supported by the Minerva Foundation, Munich. Germany, the ONR (Office of Naval Research), USA, Grant No. N00014-91-J-4104, and the Israeli Academy of Science.

[1]B. V. Weber, J. R. Boller, and R. J. Commisso, J. Appl. Phys. **45**, 1043 (1984).
[2]D. Hinshelwood, B. Weber, J. M. Grossmann, and R. J. Commisso, Phys. Rev. Lett. **68**, 3567 (1992).
[3]C. W. Mendel, Jr. and S. A. Goldstein, J. Appl. Phys. **48**, 1004 (1977).
[4]P. Ottinger, S. A. Goldstein, and R. A. Meger, J. Appl. Phys. **56**, 774 (1984).
[5]K. V. Chukbar and V. V. Yan'kov, Sov. Phys. Tech. Phys. **33**, 1293 (1988); Ya. L. Kalda and A. S. Kingsep, Sov. J. Plasma Phys. **15**, 508 (1989); A. V. Gordeev, A. V. Grechikha, A. V. Gulin, and D. M. Drozdova, Sov. J. Plasma Phys. **17**, 381 (1991).
[6]A. Fruchtman, Phys. Fluids B **3**, 1980 (1991); A Fruchtman and K. Gomberoff, *ibid.* **4**, 117 (1992); K. Gomberoff and A. Fruchtman, *ibid.* 5, 2841 (1993).
[7]A. Fruchtman and L. I. Rudakov, Phys. Rev. Lett. **69**, 2070 (1992); Phys. Rev. E **50**, 2997 (1994).
[8]R. N. Sudan and P. L. Similon, *Proceedings of the 7th International Conference on High Power Particle Beams*, Karlsruhe, Germany, 1988 (Nuclear Research Center Karlsruhe, Germany, 1988), Vol. 1, p. 416; L. I. Rudakov, C. E. Seyler, and R. N. Sudan, Comments Plasma Phys. Controlled Fusion **14**, 171 (1991).
[9]See National Technical Information Service Document No. PB92-206168 (M. Sarfaty, Ya. Krasik, R Arad, A. Weingarten, Y. Maron, and A. Fisher, in Proceedings of the 8th International Conference on High Power Particle Beams, Washington, D.C., 1992, Vol. 1, p. 633). Copies may be ordered from the National Technical Information Service, Springfield, Virginia 22161.
[10]M. Sarfaty, Y. Maron, Ya. E. Krasik, A. Weingarten, R. Arad, R. Shpitalnik, A. Fruchtman, and S. Alexiou, Phys. Plasmas, **2**, 2122 (1995).
[11]Y. Maron, E. Sarid, E. Nahshoni, and O. Zahavi, Phys. Rev. A **39**, 5856 (1989).
[12]C. W. Mendel, Jr. (private communication, 1993).